

Dual energy computed tomography quantification of carotid plaques calcification: comparison between monochromatic and polychromatic energies with pathology correlation

Lorenzo Mannelli · Lawrence MacDonald · Marcello Mancini · Marina Ferguson · William P. Shuman · Monica Ragucci · Serena Monti · Dongxiang Xu · Chun Yuan · Lee M. Mitsumori

Received: 10 July 2014 / Revised: 30 September 2014 / Accepted: 18 November 2014 / Published online: 24 December 2014
© European Society of Radiology 2014

Abstract

Purpose We compared carotid plaque calcification detection sensitivity and apparent cross-sectional area on CT as a function of CT beam energy using conventional CT techniques and virtual mono-energetic CT images generated from dual-energy acquisitions.

Methods & materials Five ex-vivo carotid endarterectomy (CEA) specimens were imaged with dual-energy computed tomography. Virtual monochromatic spectrum (VMS) CT images were reconstructed at energies between 40–140 keV. The same specimens were imaged using conventional polyenergetic spectrum (PS) CT with peak beam energies 80, 100, 120, and 140 kVp. The histological calcium areas on each corresponding CEA specimen were traced manually on digitized images of Toluidine-Blue/Basic-Fuchsin stained plastic sections.

Results 40 keV VMS CT images provided high detection sensitivity (97 %) similar to conventional PS CT images (~96 %). The calcification size measured on CT decreased systematically with increasing CT beam energy; the rate of change was larger for the VMS images than for PS images.

Conclusion From a single dual-energy CT, multiple VMS-CT images can be generated, yielding equivalent detection

sensitivity and size correlations as conventional PS-CT in CEA calcification imaging. VMS-CT at 80–100 keV provided the most accurate estimates of calcification size, as compared to histology, but detection sensitivity was reduced for smaller calcifications on these images.

Key Points

- Calcifications depicted at 80–100 keV were most similar to the histology standard.
- Conventional polychromatic images demonstrated excellent correlation with plaque size at pathology.
- Conventional polychromatic images systematically overestimate plaque size.
- Plaque calcifications can be missed on high energy monochromatic images.

Keywords Dual energy · Computed tomography · Carotid artery · Calcification · Monochromatic

Introduction

Carotid atherosclerosis can cause hemodynamic impairment in intracranial circulation as well as artery-to-artery embolisms [1]. Currently, the severity and degree of luminal stenosis are the main factors influencing therapeutic decision making in patients with atherosclerosis [2–4]. However, recent studies have revealed that plaque morphology and tissue components are important additional factors in risk assessment [5, 6]. In fact, plaques causing only minimal stenosis may still present a significant risk for distal ischemic events [7]. Evidence is building supporting the concept of the vulnerable associated with high-risk plaque in the carotid circulation, similar to coronary artery disease [8]. Therefore, noninvasive characterization of plaque composition, such as the amount of

L. Mannelli · L. MacDonald · M. Ferguson · W. P. Shuman · D. Xu · C. Yuan · L. M. Mitsumori
Departments of Radiology, University of Washington, Seattle, WA, USA

M. Mancini · M. Ragucci · S. Monti
IRCCS Fondazione SDN, Naples, Italy

L. Mannelli (✉)
Department of Radiology, Memorial Sloan Kettering Cancer Center,
1275 York Avenue, New York, NY 10065, USA
e-mail: mannellilorenzo@yahoo.it

calcification, the lipid content, the presence of necrosis or haemorrhage, neovascularization, inflammation, and thickness of the fibrous cap, can better determine the risk of stroke [9–12].

Magnetic resonance imaging (MRI), positron emission tomography (PET), and ultrasound have been used to evaluate the soft tissue component of plaque with good results; however, these techniques have significant limitations in evaluating and even visualizing the calcified portion of plaque [13–22]. Computed tomography (CT) is able to image calcifications, and it may have a specific role in evaluating this portion of the plaque [23–30].

In CT imaging, objects are examined with a polychromatic x-ray beam represented by the highest (peak) energy in the beam, e.g., 120 kVp [31]. Objects preferentially absorb x-rays with lower energy, resulting in a change in the x-ray energy spectrum [32]. The higher energy portion of the x-ray beam is what is ultimately detected [33]. Current CT systems correct this phenomenon, called beam-hardening effective energy shift, by using calibration data measured in specific phantoms and calculated with those specific functions during the image reconstruction process [34]. Polychromaticity of the x-rays causes loss of information because of energy averaging [35–37]. In dual energy CT, objects are examined with two polychromatic x-ray beams of different kVp peak energy, resulting in measurements of the linear attenuation coefficients at two different average energies. The energy dependence of x-ray absorption properties of various materials allows these two images to be used as a basis for calculating synthesized images that represent specific energy-dependent properties of the object such as different materials or different x-ray interactions (photoelectric effect vs. Compton scattering). They can also be used to synthesize images at specific energies, yielding virtual monochromatic spectral (VMS) images [38–43]. While beam-hardening still affects data acquisition of dual-energy CT, the images can yield additional information potentially useful for better tissue and morphology characterization.

Since calcium attenuation is dependent on energy level, different x-ray spectra will have different absorption by calcified plaques, potentially resulting in additional information for tissue and morphology characterization [33]. While this additional information may be derived from conventional CT that uses different polychromatic spectra (PS-CT), this is impractical because multiple scans would be required. We hypothesize that a single scan using dual-energy CT can be used to create VMS images of carotid plaque calcifications that match histology better than PS-CT techniques.

This study focuses on the evaluation of the calcific portion of atherosclerotic plaque. Thus, the objectives of this *ex vivo* study were the following:

- (1) to use human endarterectomy specimens of carotid atherosclerotic plaques to determine if changes occur in the perceived size of carotid plaque calcifications on dual-energy VMS CT images reconstructed at different energy levels (keV) and different polychromatic CT images (kVp);
- (2) to compare the size and number of carotid plaque calcifications measured via CT to histology; and [3] to quantify the change in perceived calcification size with CT beam energy (VMS and PS).

In this paper the unit ‘keV’ is used to describe the virtual monochromatic-energy of the VMS-CT images. The term ‘kVp’ is used to describe the maximum energy of a polychromatic spectrum. Thus, ‘keV’ and ‘kVp’ are associated with VMS-CT and PS-CT, respectively.

Method and materials

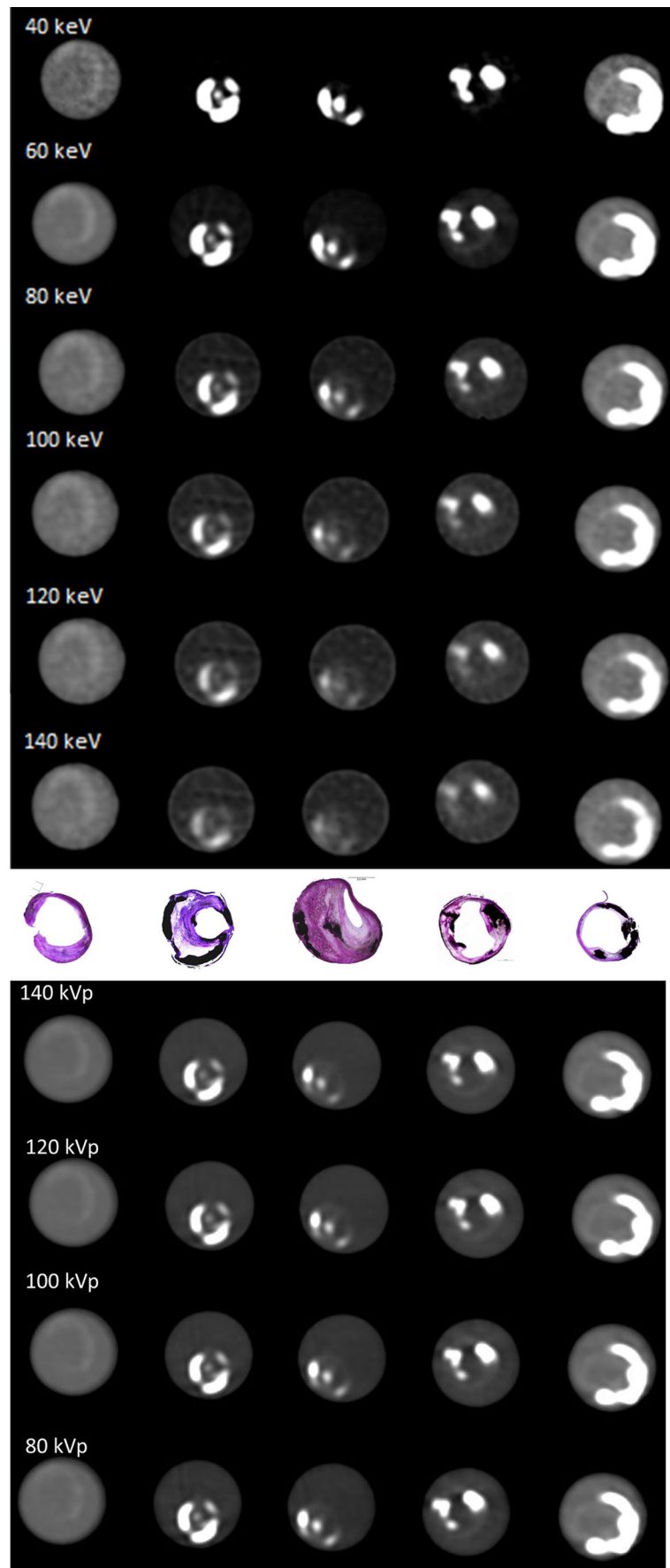
Specimens

After approval from the institutional review board, five *ex vivo* carotid endarterectomy (CEA) specimens were obtained from five patients with advanced atherosclerosis (Fig. 1). Samples were fixed in 10 % neutral buffered formalin. After CT imaging, the endarterectomy specimens were specially processed to preserve the plaque calcifications. This calcium-preserving processing required that the specimens first be embedded in plastic. Then, 8- μ m cross-sections were ground at 1-mm intervals and stained with Toluidine Blue/Basic Fuchsin to demonstrate plaque calcifications (Fig. 1). The sections were photographed and regions of calcifications were manually traced on digitized images of the sections by an experienced histopathologist blinded to the CT results [23, 44, 45]. All calcified areas on each histology slide were summed to obtain the calcification area for that slice.

CT

Each specimen was placed in formalin within a separate sample compartment and imaged with the long axis of the carotid plaques aligned with the longitudinal (z) axis. The five endarterectomy specimens were simultaneously imaged using single-source rapid tube switching dual-energy 64-channel CT (Discovery CT750 HD; GE Healthcare, Waukesha, Wisconsin, USA). Data sets were acquired with the following parameters: gantry rotation 0.6 s; detector collimation 0.625 \times 64 mm; helical pitch 0.984; field of view (FOV) 12.6 \times 12.6 cm; 640 mA; and tube voltage switching between 80 and 140 kVp with the tube voltage switched every 0.5 millisecond. The acquired dual-energy data were used to reconstruct seven VMS image sets at different energy levels (40, 60, 77, 80, 100, 120, and 140 keV). Images were reconstructed as contiguous 1-mm thick axial images with a standard kernel.

Fig. 1 Toluidine Blue/Basic Fuchsin stained section and polychromatic (140, 120, 100, 80 kVp) and reconstructed CT VMS images (40, 60, 80, 100, 120, and 100 keV) of the same location as matched by the human observer. The magnification factors are different for CT and histology



The same specimens were also imaged with a conventional polychromatic source at different tube potentials (80, 100, 120, and 140 kVp) with the same acquisition parameters as the dual energy acquisition. The dual-energy and the conventional image acquisitions were performed with the samples in the same exact position.

Image analysis

The reconstructed VMS CT axial images of the carotid plaques were then analyzed using a custom-designed computer package, CASCADE (Computer-Aided System for Cardiovascular Disease Evaluation), developed to perform quantitative analysis of plaque morphology, composition, and disease burden on cross-sectional images of diseased vessels [14, 22]. With CASCADE, the cross-sectional area of the plaque calcifications within each VMS CT image was semi-automatically measured in square millimetres using a density threshold of 130 Hounsfield units (HU) [46]. All calcified areas on each CT image slice were summed to get the calcification area for that slice.

CT and histology matching

One experienced radiologist with sub-specialty training in cardiovascular imaging matched the VMS CT images to the histology sections on the basis of the shape of the lumen, outer vessel wall, image/slice location relative to the carotid bifurcation, and the size and shape of the calcifications present in the particular image/slice of the plaque [23]. The radiologist had access to all the histological images made by the pathologist (Fig. 1b) and by scrolling through the CT images matched the CT images and histology sections [12]. The histopathologist and the radiologist analyzed the images separately with no interaction between the two. The radiologist was aware of which plaque the histological images were from, but not the level of the histological images within the plaque [23, 33].

Statistical analysis

Calcification detection sensitivity was calculated as the number seen on each CT method divided by the total number seen on the pathology slices. A Pearson correlation coefficient for a linear relationship was calculated between the pathology and CT results, and between different CT techniques. The mean difference (bias) and root-mean-square (RMS) error in CT calcification size was calculated using the calcification sizes measured via histology as the gold standard. The mean percent bias was calculated as $100 \% * (A_{CT} - A_{path}) / (A_{path})$ averaged over the calcifications found by the CT imaging technique of interest, where A_{CT} and A_{path} were the sizes (areas) of the calcifications measured by CT and pathology, respectively. Note that calcifications not seen on CT images were not used in correlation, bias, or RMSE calculations. Calcifications missing from CT scans were characterized by the detection sensitivity.

We characterized the change in the apparent size of calcifications with CT beam energy. Linear regression (least-squares minimization) was applied to the size-vs-CT beam energy data; the slope of this line indicates how fast the apparent size of the calcifications change with beam energy.

Results

All five CEA specimens studied contained plaque calcifications. Twenty to 35 sections were obtained per specimen. Figure 1 shows an example of changes in the size and appearance of plaque calcifications with different VMS energy levels and different kVp compared to histology. The areas (mm^2) of each calcification were measured via histology and on each CT image set (Fig. 1, Table 1).

A total of 146 histology sections were obtained. Nineteen sections were excluded because the carotid wall was partially damaged during plastic processing. Therefore, 127 histology sections were included in the study and matched with the corresponding CT image. Eleven slices did not contain

Table 1 The number and characteristics of the calcified plaques detected via pathology that were missed by CT are reported by X-ray energy for mono-energetic-synthesized images and for standard poly-energetic CT images.

Plaques Missed by CT	CT X-Ray Energies									
	40 Kev	60 Kev	80 Kev	100 Kev	120 Kev	140 Kev	80 kVp	100 kVp	120 kVp	140 kVp
Number	3	7	12	26	54	75	4	5	5	4
Average area at pathology (mm^2)	2.6	2.1	1.5	1.9	4.4	5.1	2	1.9	2	2.2
Average area sd (mm^2)	2	1.4	1.3	1.4	3.7	3.8	0.9	0.9	0.9	0.7
Minimal area (mm^2)	0.8	0.5	0.2	0.2	0.2	0.2	0.8	0.8	0.8	1.5
Maximal area (mm^2)	4.7	4.7	4.7	5.1	14.4	15.5	3.1	3.1	3.1	3.1

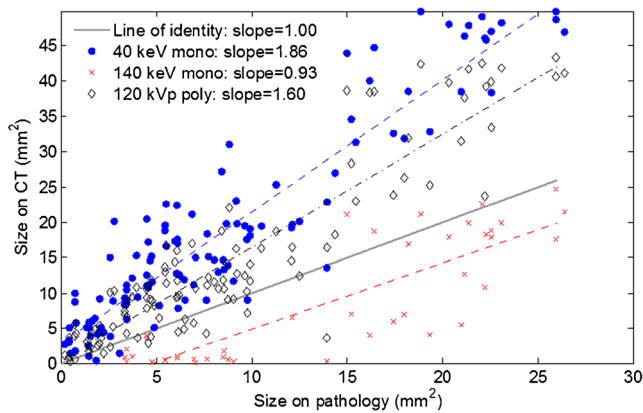


Fig. 2 Scatter plot of pathology size vs. CT size for mono-energetic CT images at 40 keV and 140 keV, and conventional 120 kVp CT image. The light gray line represents an ideal correlation between CT and pathology

calcifications as determined via pathology. There were a total of 116 slices containing one or more calcifications. The plaque calcium area per image ranged from 0.20 mm² to 26.4 mm² with a mean and median of 8.3 mm² and 6.1 mm², respectively. Unless otherwise noted, all results are cumulative across all five samples.

Figure 2 is a scatter plot of calcification area measured by histology compared to CT for three CT techniques, as follows: the highest and lowest VMS-CT energies (40 keV and 140 keV), and conventional PS-CT at 120 kVp. While there was a good statistical correlation between the calcium areas measured via histology and all of the CT image sets (Fig. 3), considerable variability is observed. By referencing the line-of-identity in Fig. 2, we see that 40 keV-VMS and 120 kVp-PS images overestimate calcification areas, while 140 keV-VMS images underestimate the calcification area.

The PS-CT image detection rate was essentially the same at 111/116 (95.7 %) for each kVp. The PS-CT images all missed the same five calcifications, with the exception of the lowest

PS-CT scan (80 kVp) that missed only four. The VMS-CT image at 40 keV missed only 3 calcifications (97.4 % detection rate); two of these three were in common with calcifications missed on the PS-CT scans. The VMS-CT detection rate decreased steadily with increasing energy. Figure 3 shows the detection rates and correlation coefficients for each CT technique as compared to pathology findings. The error bars represent the 95 % confidence interval on the correlation coefficient.

The RMS error and percent bias are shown in Fig. 4. The VMS-CT with the highest detection rate, 40 keV, also overestimated calcification sizes by ~200 %. On average, the VMS-CT bias decreases steadily with keV until the 100 keV VMS-CT image underestimated calcification size. Figure 4 shows that the lowest RMS error and percent bias occur for VMS-CT images at 80 and 100 keV. All PS-CT images overestimated calcium areas and had higher RMSE and bias than the 80 and 100 keV VMS-CTs.

The apparent size of calcifications on the VMS-CT images decreased steadily with VMS energy. This can be interpreted as causing the VMS-CT detection rate to decrease with increasing VMS energy. Small calcifications on the low energy VMS-CT images tended to disappear on higher energy images. The mean size of the 27 calcifications that were not detected on the 100 keV VMS-CT was 2.2 mm² (size on pathology), versus a mean size of 10.2 mm² (on pathology) for those detected on the 100 keV VMS-CT scan. In theory, the rate at which a calcification changes size with CT energy could be a characteristic measure of the calcification (e.g., related to the linear attenuation coefficient of the constituent material(s)). The maximum rate of change on VMS-CT images was -0.39 mm²/keV. The shrink rate tended to be larger for larger calcifications. The change in calcification size on PS-CT images was very small, with a maximum absolute value in our sample of 0.13 mm²/kVp.

Fig. 3 Correlation coefficient (ρ light gray) between calcification sizes found by pathology and CT imaging using different CT techniques. The error bars represent the 95 % CI on ρ . CT detection rate of calcifications (dark gray bars) is the fraction of calcifications seen on pathology that were also identified on CT images. Using 140 keV VMS, only 35 % of the slices containing calcifications at pathology were detected (see also table 1)

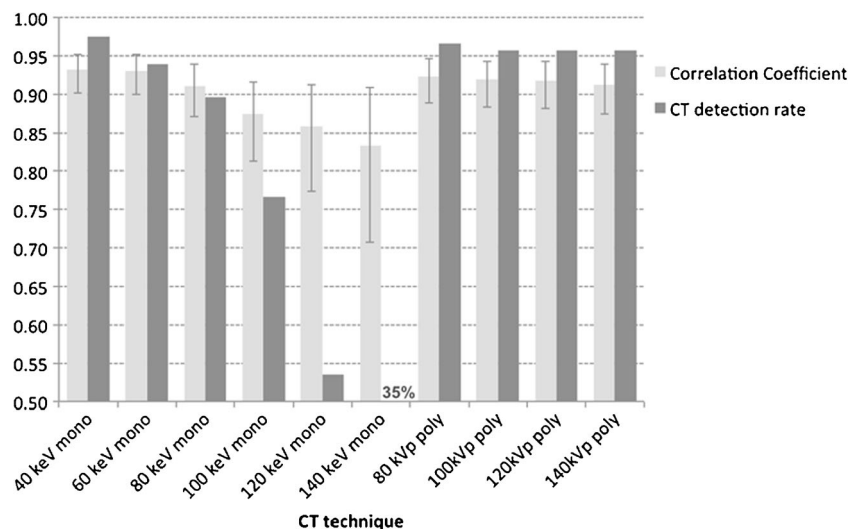
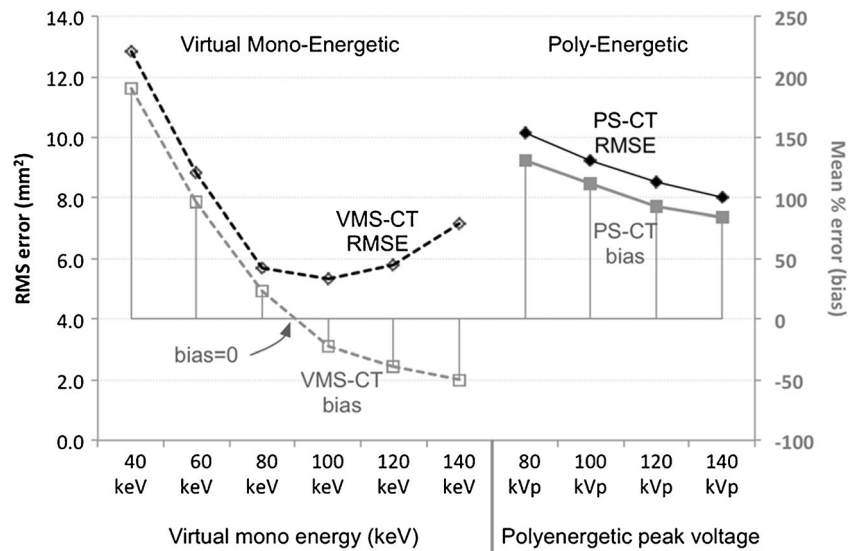


Fig. 4 Root-mean-square error (RMSE) and mean percent (%) error of calcifications sizes measured at CT for the different x-ray energies, with sizes measured on pathology taken as the true size



Discussion

In this study we used dual-energy CT imaging to generate VMS CT images of five CEA specimens (Fig. 1), with the goal of estimating the size and number of calcifications and comparing the results to conventional PS CT images and pathological results. For the *ex vivo* experimental conditions used here, and using histology as the gold standard, we demonstrated the following: [1] The size and number of plaque calcifications measured on VMS-CT images depended on the energy level used for the image reconstruction, whereas on PS-CT images there was very little dependence on x-ray beam peak energy (kVp) (Fig. 3); [2] The calcification detection rate and size estimation was better for VMS-CT than for PS-CT, although detection and size estimation were optimized at a different energy VMS (detection sensitivity was optimized at 40 keV, size estimation was optimized between 80-100 keV) (Figs. 3, 4); and [3] Related to above, the apparent calcification size on VMS-CT images decreased steadily with an increasing keV (Fig. 5), revealing it was smaller calcifications that were not detected on higher keV VMS-CT images where lower detection sensitivity was

observed. The missed calcifications were smaller on average, but calcifications as large as 15 mm² (as measured by pathology) were missed on the 140 keV VMS-CT image.

By interpolating findings between 80 keV VMS-CTs, which overestimate calcification size, and 100 keV VMS-CTs that underestimate size, we believe a zero mean bias could be achieved with a 90 keV VMS-CT; however, the estimate would still carry a RMSE of ~6 mm (Fig. 4). This result applies to the samples scanned alone, and these results would likely change when examining carotid calcifications in vivo.

Calculating how calcifications or other plaque features change apparent size with VMS energy is easily done from multiple VMS-CT images synthesized from a dual-energy CT. This metric is not practical for PS-CT, as it would require multiple scans.

Figure 3 shows the high correlation coefficients between CT and pathology calcification sizes. Figures 2 and 4, however, show that, despite the high correlation coefficient, there is still considerable variability in the relationship between calcification sizes. For example, while the vast majority of calcifications seen on low energy VMS-CT images and on PS-CT images were larger than measured via pathology, a few were also smaller on CT images than as determined by

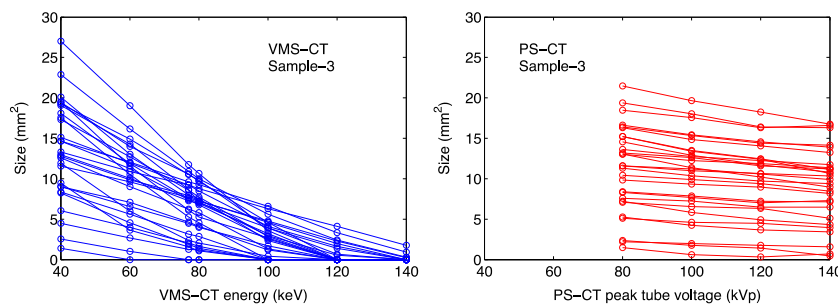


Fig. 5 Calcification sizes vs. CT x-ray beam energy for CEA sample 3. Each line shows the change in apparent calcification size for each image slice of sample 3. Linear regression (least-squares minimization) was applied to non-zero data to measure how fast apparent calcification size

changed: across all 5 samples, calcifications shrank at rates between -0.06 and -0.39 mm²/keV on VMS-CT images, whereas the size change was only -0.01 to -0.13 mm²/kVp for PS-CT images

pathology in the same images (Fig. 2, markers below the line of identity). The PS-CT images all overestimate calcification size substantially (percent bias, Fig. 4). This is probably due to inadequate correction of effective energy shift causing the beam-hardening phenomenon in the regions peripheral to calcific atherosclerotic plaques [17, 37, 38]. VMS-CT images at a low keV also suffer from beam-hardening and ‘blooming’ common to PS-CT images, but VMS CT images seem to be able to recover this information [35] at a higher VMS energy. As mentioned above, higher VMS energy examinations have reduced calcification detection sensitivity. However, when using dual-energy CT imaging, VMS-CT at several energies can be reconstructed from a single dual-energy scan; thus, a VMS-CT image that optimizes detection rate, and another that optimizes size estimation can both be generated. An obvious limitation is that the size cannot be estimated for those calcifications that are not detected on the higher energy VMS image. Further analysis of the differences in image characteristics between VMS CT images at different energies could potentially provide additional information on the plaque density and calcium distribution within the calcification. For example, use of low energy levels could increase the imaging sensitivity for small plaque calcifications, while high energy levels could reduce the effects of calcium blooming artefacts, which can obscure the vessel lumen and mask other important plaque components [12].

We used an HU threshold of 130 based on that value being used for coronary artery calcium scoring [45]. Our results did not change for thresholds of 120 HU or 140 HU on two samples where these thresholds were applied. HUs are defined for PS-CT with respect to water and air linear attenuation coefficients for a PS x-ray beam. An examination of the appropriate units for the analysis of VMS-CT images is required. The apparent size of calcifications on VMS-CT images will be thresholddependent with the proper selection of units and range of thresholds. We also used the same convolution filter for all image reconstruction; however, the use of different convolution filters may have an effect on carotid plaque attenuation values [47]. It remains to be determined which convolution filter can optimize carotid plaque size when using VMS images.

This study had several limitations. First, this was an ex vivo study; therefore, further work is needed to establish whether the results apply to in vivo situations. Second, although the number of slices evaluated was high, the total number of carotid samples was small. Third, imperfect matching of plaque slices between pathology and CT images may have led to an increased variance in the results. Lastly, evaluation of the non-calcified portion of the plaques has not been attempted.

There are fundamental challenges in using imaging to measuring quantitative parameters in structures that have dimensions smaller than 2-3 times the intrinsic spatial resolution of the imaging system. In this case, voxel ‘spill-over,’ or voxel partial volume effect, leads to material mixing between

adjacent image voxels. The very small calcifications in carotid arteries fall within this limit of smaller than 2-3 times the intrinsic CT spatial resolution. The observed change of calcification size with VMS-CT energy is in part due to inherent and potentially informative properties of the calcification. However, other effects are also at play, including the voxel partial volume effect and, in practice, variability in background conditions (e.g., neck size). These effects could be difficult to calibrate for in in vivo imaging.

In conclusion, there was a high correlation between calcification sizes measured via CT and pathology, but broad variability as measured by the RMSE between the two measurements persisted. VMS-CT images at 80-100 keV had the lowest bias and RMSE for the ex vivo experiments conducted here. The PS-CT images had 95.7 % calcification detection sensitivity, but overestimated calcification size by ~100 %, both nearly independent of peak x-ray beam energy. Results of VMS-CT images were strongly dependent on the (virtual) x-ray energy; the 40 keV VMS-CT had a 97.4 % detection sensitivity but overestimated size by ~200 %, whereas the VMS-CTs with the smallest bias and RMSE, 80 and 100 keV, had only 89.7 % and 76.7 % detection sensitivities, respectively.

We demonstrated that plaque calcifications were missed on higher energy monochromatic images; we speculate that this is likely dependent on two factors, plaque size and total calcium content. The fact that analysis of the plaque size changes using different VMS images could provide additional information on the composition of the calcified portion of the carotid plaque; however, this approach must be validated under in vivo imaging conditions and faces fundamental challenges for the calcifications that are comparable in size to the intrinsic spatial resolution of CT. Dual-energy image data can also be used to generate virtual material composition images (as opposed to virtual monochromatic beam energy images). Evaluation of plaque calcium content using virtual material decomposition is another promising approach [48].

Acknowledgments The scientific guarantor of this publication is Lee M Mitsumori. The authors of this manuscript declare no relationships with any companies whose products or services may be related to the subject matter of the article. The authors state that this work has not received any funding. Lawrence MacDonald, one of the authors, has significant statistical expertise. Institutional review board approval was obtained. Written informed consent was obtained from all subjects (patients) in this study. No animals were included in this study. Some study subjects or cohorts have been previously reported in *Eur Radiol* (2013) 23:367-374. Methodology: prospective, experimental, performed at one institution.

References

1. Gasecki AP, Hachinski VC, Mendel T, Barnett HT (1992) Endarterectomy for symptomatic carotid stenosis. Review of the European and North American Symptomatic Carotid Surgery Trials. *Nebraska Med J* 77:121–123

2. Rijbroek A, Wisselink W, Vriens EM, Barkhof F, Lammertsma AA, Rauwerda JA (2006) Asymptomatic carotid artery stenosis: past, present and future. How to improve patient selection? *Eur Neurol* 56:139–154
3. Barnett HJ, Taylor DW, Eliasziw M et al (1998) Benefit of carotid endarterectomy in patients with symptomatic moderate or severe stenosis. North American Symptomatic Carotid Endarterectomy Trial Collaborators. *N Engl J Med* 339:1415–1425
4. Bowen BC, Quencer RM, Margosian P, Pattany PM (1994) MR angiography of occlusive disease of the arteries in the head and neck: current concepts. *AJR Am J Roentgenol* 162:9–18
5. Carr JC, Shaibani A, Russell E, Finn JP (2001) Contrast-enhanced magnetic resonance angiography of the carotid circulation. *Top Magn Reson Imaging TMRI* 12:349–357
6. Chen H, Li F, Zhao X, Yuan C, Rutt B, Kerwin WS (2011) Extended graphical model for analysis of dynamic contrast-enhanced MRI. *Magn Reson Med Off J Soc Magn Reson in Med / Soc Magn Reson Med* 66:868–878
7. North American Symptomatic Carotid Endarterectomy Trial C (1991) Beneficial effect of carotid endarterectomy in symptomatic patients with high-grade carotid stenosis. *N Engl J Med* 325:445–453
8. Owen DR, Lindsay AC, Choudhury RP, Fayad ZA (2011) Imaging of atherosclerosis. *Annu Rev Med* 62:25–40
9. Mannelli L, Cherian V, Nayar A, Srichai-Parsia M (2012) Loeffler's endocarditis in hypereosinophilic syndrome. *Curr Probl Diagn Radiol* 41:146–148
10. Demarco JK, Ota H, Underhill HR et al (2010) MR carotid plaque imaging and contrast-enhanced MR angiography identifies lesions associated with recent ipsilateral thromboembolic symptoms: an in vivo study at 3T. *AJNR Am J Neuroradiology* 31:1395–1402
11. Bryan RN, Drewyer RG, Gee W (1978) Separate origins of the left internal and external carotid arteries from the aorta. *AJR Am J Roentgenol* 130:362–365
12. Barreto M, Schoenhagen P, Nair A et al (2008) Potential of dual-energy computed tomography to characterize atherosclerotic plaque: ex vivo assessment of human coronary arteries in comparison to histology. *J Cardiovasc Comput Tomogr* 2:234–242
13. Waaijjer A, Weber M, van Leeuwen MS et al (2009) Grading of carotid artery stenosis with multidetector-row CT angiography: visual estimation or caliper measurements? *Eur Radiol* 19:2809–2818
14. Saba L, Anzidei M, Marincola BC, et al. Imaging of the Carotid Artery Vulnerable Plaque. *Cardiovascular and interventional radiology*. 2013.
15. Myers KS, Rudd JH, Hailman EP et al (2012) Correlation between arterial FDG uptake and biomarkers in peripheral artery disease. *J Am Coll Cardiol Img* 5:38–45
16. Underhill HR, Yarnykh VL, Hatsukami TS et al (2008) Carotid plaque morphology and composition: initial comparison between 1.5- and 3.0-T magnetic field strengths. *Radiology* 248:550–560
17. Miralles M, Merino J, Busto M, Perich X, Barranco C, Vidal-Barraquer F (2006) Quantification and characterization of carotid calcium with multi-detector CT-angiography. *Eur J Vasc Endovasc Surg Off J Eur Soc Vasc Surg* 32:561–567
18. Balu N, Wang J, Dong L, Baluyot F, Chen H, Yuan C (2009) Current techniques for MR imaging of atherosclerosis. *Top Magn Reson Imaging TMRI* 20:203–215
19. Briley-Saebo KC, Mulder WJ, Mani V et al (2007) Magnetic resonance imaging of vulnerable atherosclerotic plaques: current imaging strategies and molecular imaging probes. *J Magn Reson Imaging JMRI* 26:460–479
20. Bucerius J, Mani V, Moncrieff C et al (2012) Impact of noninsulin-dependent type 2 diabetes on carotid wall 18F-fluorodeoxyglucose positron emission tomography uptake. *J Am Coll Cardiol* 59:2080–2088
21. Mannelli L, Mosca R, Henry G, Srichai-Parsia MB (2011) A case of berry syndrome type 2B. *Congenit Heart Dis* 6:389–392
22. Kerwin W, Xu D, Liu F et al (2007) Magnetic resonance imaging of carotid atherosclerosis: plaque analysis. *Top Magn Reson Imaging TMRI* 18:371–378
23. Hoffmann U, Kwait DC, Handwerker J, Chan R, Lamuraglia G, Brady TJ (2003) Vascular calcification in ex vivo carotid specimens: precision and accuracy of measurements with multi-detector row CT. *Radiology* 229:375–381
24. de Weert TT, Ouhlous M, Meijering E et al (2006) In vivo characterization and quantification of atherosclerotic carotid plaque components with multidetector computed tomography and histopathological correlation. *Arterioscler Thromb Vasc Biol* 26:2366–2372
25. Fleischmann D, Boas FE (2011) Computed tomography—old ideas and new technology. *Eur Radiol* 21:510–517
26. Hoang MV, Linnau KF, Gill EA, Lehnert BE, Mannelli L (2012) Computed tomography diagnosis of myocardial infarction in a patient with normal initial cardiac biomarkers. *Emerg Radiol* 19:75–78
27. Mannelli L, Caldwell JH, Elman S (2013) Lewis DH. Do BW, Vesselle H. Multiple-Gated Acquisition Scan With Normal Left Ventricular Ejection Fraction and LBBB. *Clinical nuclear medicine*
28. Knollmann FD, Helmig K, Kapell S et al (2003) Coronary artery calcium scoring: diagnostic accuracy of different software implementations. *Investig Radiol* 38:761–768
29. Relucenti M, Heyn R, Petruzzello L, Pugliese G, Taurino M, Familiari G (2010) Detecting microcalcifications in atherosclerotic plaques by a simple trichromic staining method for epoxy embedded carotid endarterectomies. *Eur J Histochem EJH* 54:e33
30. Korn A, Bender B, Brodoefel H, et al. Grading of Carotid Artery Stenosis in the Presence of Extensive Calcifications: Dual-Energy CT Angiography in Comparison with Contrast-Enhanced MR Angiography. *Clinical neuroradiology*. 2013.
31. Galonska M, Ducek F, Kertesz-Zborilova T, Meyer R, Guski H, Knollmann FD (2008) Characterization of atherosclerotic plaques in human coronary arteries with 16-slice multidetector row computed tomography by analysis of attenuation profiles. *Acad Radiol* 15:222–230
32. Renker M, Nance JW Jr, Schoepf UJ et al (2011) Evaluation of heavily calcified vessels with coronary CT angiography: comparison of iterative and filtered back projection image reconstruction. *Radiology* 260:390–399
33. Mannelli L, Mitsumori LM, Ferguson M et al (2013) Changes in measured size of atherosclerotic plaque calcifications in dual-energy CT of ex vivo carotid endarterectomy specimens: effect of monochromatic keV image reconstructions. *Eur Radiol* 23:367–374
34. Tran DN, Straka M, Roos JE, Napel S, Fleischmann D (2009) Dual-energy CT discrimination of iodine and calcium: experimental results and implications for lower extremity CT angiography. *Acad Radiol* 16:160–171
35. Kalender WA, Perman WH, Vetter JR, Klotz E (1986) Evaluation of a prototype dual-energy computed tomographic apparatus. I. *Phantom Stud Med Phys* 13:334–339
36. Matsumoto K, Jinzaki M, Tanami Y, Ueno A, Yamada M, Kuribayashi S (2011) Virtual monochromatic spectral imaging with fast kilovoltage switching: improved image quality as compared with that obtained with conventional 120-kVp CT. *Radiology* 259:257–262
37. Menvielle N, Goussard Y, Orban D, Soulez G (2005) Reduction of Beam-Hardening Artifacts in X-Ray CT. *Conf Proc Ann Int Conf IEEE Eng Med Biol Soc IEEE Eng Med Biol Soc Conf* 2:1865–1868
38. Sun H, Qiu S, Lou S, Liu J, Li C, Jiang G (2004) A correction method for nonlinear artifacts in CT imaging. *Conf Proc Ann Int Conf IEEE Eng Med Biol Soc IEEE Eng Med Biol Soc Conf* 2:1290–1293
39. Idris AE, Fessler JA (2003) Segmentation-free statistical image reconstruction for polyenergetic x-ray computed tomography with experimental validation. *Phys Med Biol* 48:2453–2477
40. Flohr TG, McCollough CH, Bruder H et al (2006) First performance evaluation of a dual-source CT (DSCT) system. *Eur Radiol* 16:256–268

41. Alvarez RE, Macovski A (1976) Energy-selective reconstructions in X-ray computerized tomography. *Phys Med Biol* 21:733–744
42. Elbakri IA, Fessler JA (2002) Statistical image reconstruction for polyenergetic X-ray computed tomography. *IEEE Trans Med Imaging* 21:89–99
43. Srichai MB, Lim RP, Donnino R et al (2012) Low-dose, prospective triggered high-pitch spiral coronary computed tomography angiography: comparison with retrospective spiral technique. *Acad Radiol* 19:554–561
44. Langheinrich AC, Kampschulte M, Crossmann C et al (2009) Role of computed tomography voxel size in detection and discrimination of calcium and iron deposits in atherosclerotic human coronary artery specimens. *J Comput Assist Tomogr* 33:517–522
45. Sarwar A, Rieber J, Mooyaart EA et al (2008) Calcified plaque: measurement of area at thin-section flat-panel CT and 64-section multidetector CT and comparison with histopathologic findings. *Radiology* 249:301–306
46. de Weert TT, de Monye C, Meijering E et al (2008) Assessment of atherosclerotic carotid plaque volume with multidetector computed tomography angiography. *Int J Cardiovasc Imaging* 24:751–759
47. Cademartiri F, La Grutta L, Runza G et al (2007) Influence of convolution filtering on coronary plaque attenuation values: observations in an ex vivo model of multislice computed tomography coronary angiography. *Eur Radiol* 17:1842–1849
48. Johnson TR, Krauss B, Sedlmair M et al (2007) Material differentiation by dual energy CT: initial experience. *Eur Radiol* 17:1510–1517